Improved approach to spin-polarized relativistic LMTO formalism: Application to the electronic structure of Fe-Ni compounds at the Earth's core conditions

A. E. Krasovskii
Institute of Magnetism, Ukrainian NAS, 252680, Kiev 142, Ukraine
(Received 17 March 1999)

A first-principles fully relativistic spin-polarized linear muffin-tin orbital method for calculations of electronic structure of magnetic crystals that contain heavy elements is presented. The orbital contribution to the four-current density is omitted, and no further approximation is made to treat the spin polarization and the spin-orbit coupling effects in solving the Dirac equation for a spin-dependent potential. The self-consistent band structure and calculated spin and orbital magnetic moments for Fe metal are compared with previous calculations and with experimental data. First-principles non-spin-polarized calculations of the ground state of some ordered Fe-Ni alloys at the Earth's core pressure for several concentrations of Fe are presented. In the density-of-states function of the nonmagnetic $FeNi_3$ a pronounced peak in the vicinity of the Fermi level has been observed. A spin-polarized calculation for $FeNi_3$ has been performed, which predicts a weak ferromagnetism of $0.393\mu_B$/cell. The effect is explained in terms of the electronic structure. An attempt is made to roughly estimate the Curie temperature for this compound. [S0163-1829(99)11741-7]

I. INTRODUCTION

The local-spin density approximation (LSDA) with gradient corrections is known to provide a reasonable description of the ground-state properties of the majority of metallic compounds. However, important physical phenomena, such as magnetocrystalline anisotropy, Kerr effect, or the ground-state properties of materials containing heavy elements under high pressure, require accurate treatment of both magnetic and relativistic effects.

Within the nonperturbational approach to the problem the following generalizations of classical band-structure methods to treat ''on equal footing'' both the spin-polarization and the relativistic effects have been developed: the linear muffin-tin orbital (LMTO) method,[1] the augmented spherical wave (ASW) method,[2] the cellular method,[3] and Korringa-Kohn-Rostoker (KKR) method.[4] Linear band-structure methods, LMTO and ASW, are about a hundred times faster than KKR, and the accuracy of eigenvalues and eigenfunctions remains sufficiently high. Apart from the neglect of a weak coupling between the states with $\Delta l = \pm 2$, $\Delta j = \pm 1$ (Refs. 5 and 6) the relativistic spin-polarized generalizations contain certain approximations that make it technically possible to solve the Kohn-Sham-Dirac equations in the presence of the magnetic field. An aim of the present paper is to generalize the conventional relativistic LMTO method[7] (RLMTO) in order to incorporate the spin polarization effects with explicitly taking into account the off-diagonal elements of the single-site transition matrix.[6,8]

One of the most important unresolved problems of geochemistry is the chemical composition, structural, and magnetic properties of the Earth's interior. In this paper we make an attempt to coherently understand the structure of the Earth's core on the basis of *ab initio* calculations of Fe-Ni alloys.

It is generally accepted that the composition of the Earth's core (and also other planets) should be similar to one of the siderites, i.e., iron-nickel alloy based meteorites that contain, on the average, 90% Fe and 10% Ni. Amongst abundant chemical elements in space only iron and nickel can lead to the observed averaged density of the planets in the solar system. The Earth's core consists of two layers: the solid inner core (IC) with the radius of 1250 km and the liquid outer core (OC), a layer from 1250 to 3470 km. Modern geophysical data give the following estimates of the IC conditions: the pressure is between 3 and 4 Mbar, the temperature between 4000 and 8000 K, and the density between 13 and 17 g/cm^3 (Ref. 9).

Though possible distribution of nickel through the Earth's core is not known, it is believed that the core contains mostly iron, which is the basis for modern theoretical solid-state models of the IC. However, the uncertainty in the chemical composition makes the results ambiguous. Recently attempts have been made to elucidate the structure of the IC by considering the behavior of pure iron under very high pressures up to 4 Mbar both experimentally[10] and theoretically.[11] It has been established that all possible high-pressure close-packed phases of iron are nonmagnetic. The Fe-Ni alloys at IC pressures has been experimentally studied by Mao *et al.*[12]

However, more than 30 years ago it has been found that in the pressure range from 1.5 to 3 Mbar the density of nickel is about 7% larger than the density of iron.[13] That is not very surprising because the electronic structures of the two neighboring transition metals should not differ significantly under extreme pressures, and, therefore, the difference in the densities should result from the difference of their atomic weights, which is about 5%. This suggests that IC may be enriched by nickel (because that minimizes the gravitation energy), thereby making it necessary to consider also Ni-based alloys. Note that the 10% content of nickel is a value averaged over the whole core (including both OC and IC), and the amount is sufficient to fill the IC with pure nickel.

Although little is known about the crystal structure of the IC, previous studies[11] have shown that at the IC conditions pure iron can crystallize *only* in close-packed structures (e.g., fcc, hcp, and dhcp). The result is natural for the nearly twofold-compressed iron. Nevertheless, at extreme pressures interatomic distances may become so small that the outer core shells overlap (Fe $3p$ states). In that case the above conclusion that the crystal structure should be close-packed may become incorrect.

Based on the above arguments we start with the assumption that at least one spherical layer of the IC may contain the iron-nickel alloy with the chemical composition of $FeNi_3$. In this work we consider only crystallographically ordered alloys. Also, this compound should possess the close-packed crystal structure of Cu_3Au type that originates from the fcc structure of pure Ni and $Fe_{1-x}Ni_x$ alloys with $x>0.2$,[14] with Fe atoms occupying the cube corners and Ni atoms the face centers. Thus the mass density of the compound corresponds to the estimated density of the IC, which is 13 g/cm^3 and leads to the lattice constant of 5.847 a.u. (3.094 Å). Note that at atmospheric pressure and room temperature the lattice constant of $FeNi_3$ is 8.862 a.u.,[15] so the volume compression by a factor of about 1.5 will be studied.

At first sight it seems that in extremely compressed $FeNi_3$ iron behaves very similarly to nickel. However, according to non-spin-polarized electronic structure calculations the density-of-states (DOS) function of $FeNi_3$ exhibits a pronounced peak in the vicinity of the Fermi level. The DOS at the Fermi energy, E_F, is rather large [$N(E_F)=6.4$ states/eV atom], and, according to the Stoner model of ferromagnetism, a spin alignment may occur at least at $T=0$. This makes it interesting to perform spin-polarized ground-state band-structure calculations of the alloy. We have found that the spin alignment is favorable, the resulting magnetic moment being $0.393\mu_B$/cell. In addition, we make an attempt to roughly estimate the Curie temperature of this compound on the basis of the Stoner theory.

The basic formalism of the spin-polarized relativistic linear muffin-tin orbital method is presented in Sec. II. An application of the computational scheme to the self-consistent band-structure calculation of iron is presented in Sec. III. The results are compared with previous calculations and with available experimental data. The results on the electronic structure of the ordered Fe-Ni alloys at the inner Earth's core conditions are presented in Sec. IV. Section V concludes the paper.

II. SPIN-POLARIZED RELATIVISTIC LINEAR MUFFIN-TIN ORBITAL METHOD

The most widely used approach to treat both relativistic effects and the effect of the magnetic field on electrons in a solid is based on a scheme proposed by MacDonald and Vosko.[16] In this approach the Dirac equation for a spin-dependent potential has the form

$$[\mathcal{H}(\mathbf{r})-E]\psi(\mathbf{r})=0, \tag{1}$$

$$\mathcal{H}(\mathbf{r})=\mathcal{H}^0(\mathbf{r})+\mathcal{H}^M(\mathbf{r}), \tag{2}$$

$$\mathcal{H}^0(\mathbf{r})=c\boldsymbol{\alpha}\cdot\mathbf{p}+\beta mc^2+IV(\mathbf{r}), \tag{3}$$

$$V(\mathbf{r})=V^H(\mathbf{r})+V^{xc}(\mathbf{r}), \tag{4}$$

where $\mathcal{H}^0(\mathbf{r})$ is the Dirac operator, $\boldsymbol{\alpha}$ and β are the standard Dirac matrices, and I is the unity matrix. The spin-dependent part of the Hamiltonian,

$$\mathcal{H}^M(\mathbf{r})=\beta\boldsymbol{\sigma}\cdot\mathbf{B}(\mathbf{r}), \tag{5}$$

contains an effective magnetic field $\mathbf{B}(\mathbf{r})$,

$$\mathbf{B}(\mathbf{r})=\mu_B[\mathbf{B}^{xc}(\mathbf{r})+\mathbf{B}^{ext}(\mathbf{r})], \quad \mu_B=\frac{e\hbar}{2mc}, \tag{6}$$

which couples to the spin of the electron. Here $\mathbf{B}^{ext}$ is an external field. The superscripts H and xc refer to the Hartree and the exchange-correlation potentials, respectively,

$$V^{xc}(\mathbf{r})=\frac{\delta}{\delta n}E^{xc}[n,\mathbf{m}], \quad \mathbf{B}^{xc}(\mathbf{r})=\frac{\delta}{\delta \mathbf{m}}E^{xc}[n,\mathbf{m}], \tag{7}$$

where $n(\mathbf{r})$ and $\mathbf{m}(\mathbf{r})$ are the electron and the spin magnetization densities, respectively.

Each atom is surrounded by a so-called atomic sphere inside which the potential is thought to be spherically symmetric. Inside the sphere the bispinor solutions of Eq. (1) are given by a general spin-angular expansion,

$$\psi_{\kappa\mu}(E,\mathbf{r})=\sum_{\kappa'\mu'}\begin{bmatrix} g^{\mu'\mu}_{\kappa'\kappa}(E,r)\chi^{\mu'}_{\kappa'}(\hat{r}) \\ if^{\mu'\mu}_{\kappa'\kappa}(E,r)\chi^{\mu'}_{-\kappa'}(\hat{r}) \end{bmatrix}. \tag{8}$$

$\chi^{\mu}_{\kappa}(\hat{r})$ are the spin-angular functions and κ is the relativistic quantum number. As has been established in Refs. 5 and 6, for spherically averaged potentials $V(\mathbf{r})$ and $\mathbf{B}(\mathbf{r})$, Eq. (1) results in an infinite set of coupled equations for radial functions. The usual approximation is to neglect the weak spin-orbit coupling of the order of $(1/c^2)(1/r)[dB(r)/dr]$ between the states with $\Delta l=\pm 2$, $\Delta j=\pm 1$ and to keep only the coupling between the states with $\Delta l=0$, $\Delta j=\pm\frac{1}{2}$ so that the infinite set decomposes into independent sets of four (for $|\mu|\leq l-\frac{1}{2}$) or two (for $|\mu|=l+\frac{1}{2}$) coupled equations for each $l\mu$.

Using the notation

$$\kappa=\begin{Bmatrix} s \\ l \end{Bmatrix}=\begin{cases} -l-1=-j-\frac{1}{2}<0 & \text{if } s=+\frac{1}{2} \\ l=j+\frac{1}{2}>0 & \text{if } s=-\frac{1}{2} \end{cases} \tag{9}$$

one can rewrite Eq. (8) for $|\mu|\leq l-\frac{1}{2}$ in terms of two linearly independent basic solutions of Eq. (1),[4]

$$\psi_{l\mu}(E,\mathbf{r})=\sum_{\eta=1,2}c^{\eta}_{l\mu}\phi^{\eta}_{l\mu}(E,\mathbf{r}), \tag{10}$$

where coefficients $a^{\eta}_{l\mu}$ depend on boundary conditions so as to match to the solutions outside the atomic sphere. Here

$$\phi^{\eta}_{l\mu}(E,\mathbf{r})=\sum_{s=\pm\frac{1}{2}}\varphi^{s,\eta}_{l\mu}(E,\mathbf{r}), \tag{11}$$

where the partial solution takes the form

$$\varphi^{s,\eta}_{l\mu}(E,\mathbf{r})=i^l\begin{bmatrix} g^{s,\eta}_{l\mu}(E,r)\chi^{s}_{l,\mu}(\hat{r}) \\ if^{s,\eta}_{l\mu}(E,r)\chi^{-s}_{l+2s,\mu}(\hat{r})\end{bmatrix}. \tag{12}$$

The energy derivative of the partial solution is introduced in a standard manner

$$\dot{\varphi}^{s,\eta}_{l\mu}(E,\mathbf{r})=i^l\begin{bmatrix} \dot{g}^{s,\eta}_{l\mu}(E,r)\chi^{s}_{l,\mu}(\hat{r}) \\ i\dot{f}^{s,\eta}_{l\mu}(E,r)\chi^{-s}_{l+2s,\mu}(\hat{r})\end{bmatrix}. \tag{13}$$

It is easy to obtain the standard set of the relations[17,7]

$$(\mathcal{H}-E)\,\phi^{\eta}_{l\mu}(E,\mathbf{r})=0, \tag{14}$$

$$(\mathcal{H}-E)\,\dot{\phi}^{\eta}_{l\mu}(E,\mathbf{r})=\phi^{\eta}_{l\mu}(E,\mathbf{r}), \tag{15}$$

$$\langle\phi^{\eta'}_{l'\mu'}(E,\mathbf{r})|\phi^{\eta}_{l\mu}(E,\mathbf{r})\rangle=\delta_{\eta'\eta}\delta_{l'l}\delta_{\mu'\mu}, \tag{16}$$

$$\forall\,\eta',\eta\quad\langle\phi^{\eta'}_{l\mu}(E,\mathbf{r})|\dot{\phi}^{\eta}_{l\mu}(E,\mathbf{r})\rangle=0. \tag{17}$$

The Dirac equation (1) for free-electron states with $E-V-\beta\boldsymbol{\sigma}\cdot\mathbf{B}=0$ has two bispinor solutions:[7] the solution singular at the origin

$$\tilde{\phi}^{s}_{l\mu}(D=-l-1,\mathbf{r}) =i^l\begin{bmatrix} \left(\frac{r}{S}\right)^{-l-1}\chi^{s}_{l,\mu}(\hat{r}) \\ -i\,\theta(s)\frac{2l+1}{cS}\left(\frac{r}{S}\right)^{-l-2}\chi^{-s}_{l+2s,\mu}(\hat{r})\end{bmatrix}, \tag{18}$$

where D is a logarithmic derivative, and the regular one

$$\tilde{\phi}^{s}_{l\mu}(D=l,\mathbf{r})=i^l\begin{bmatrix} \left(\frac{r}{S}\right)^{l}\chi^{s}_{l,\mu}(\hat{r}) \\ +i\,\theta(-s)\frac{2l+1}{cS}\left(\frac{r}{S}\right)^{l-1}\chi^{-s}_{l+2s,\mu}(\hat{r})\end{bmatrix}. \tag{19}$$

Here the tilde refers to free electrons, and S is the radius of the atomic sphere.

Therefore the solution of Eq. (1) inside the sphere is chosen as

$$\Psi(E,\mathbf{r})=\sum_{ls\mu}\sum_{\eta=1,2}c^{\eta}_{l\mu}\varphi^{s,\eta}_{l\mu}(E,\mathbf{r}), \tag{20}$$

and, similarly to the conventional RLMTO method,[7] the expression for the wave function with an arbitrary logarithmic derivative D reads

$$\Phi^{s}_{l\mu}(D,\mathbf{r})=\sum_{\eta}\,[a^{\eta}_{l\mu}(D)\varphi^{s,\eta}_{l\mu}(E_\nu,\mathbf{r})+b^{\eta}_{l\mu}(D)\dot{\varphi}^{s,\eta}_{l\mu}(E_\nu,\mathbf{r})]. \tag{21}$$

Similarly to the procedure of Ebert[1] the functions (21) are matched smoothly to the Neumann (18) and Bessel (19) solutions to obtain a set of four equations for every logarithmic derivative $D=\{-l-1,l\}$.

$$\sum_{\eta}\,[a^{\eta}_{l\mu}(D)g^{+1/2,\eta}_{l\mu}(S)+b^{\eta}_{l\mu}(D)\dot{g}^{+1/2,\eta}_{l\mu}(S)]=1,$$

$$\sum_{\eta}\,[a^{\eta}_{l\mu}(D)f^{+1/2,\eta}_{l\mu}(S)+b^{\eta}_{l\mu}(D)\dot{f}^{+1/2,\eta}_{l\mu}(S)] =\begin{cases} -\dfrac{2l+1}{cS} & \text{if } D=-l-1 \\ 0 & \text{if } D=l,\end{cases}$$

$$\sum_{\eta}\,[a^{\eta}_{l\mu}(D)g^{-1/2,\eta}_{l\mu}(S)+b^{\eta}_{l\mu}(D)\dot{g}^{-1/2,\eta}_{l\mu}(S)]=1,$$

$$\sum_{\eta}\,[a^{\eta}_{l\mu}(D)f^{-1/2,\eta}_{l\mu}(S)+b^{\eta}_{l\mu}(D)\dot{f}^{-1/2,\eta}_{l\mu}(S)] =\begin{cases} 0 & \text{if } D=-l-1 \\ +\dfrac{2l+1}{cS} & \text{if } D=l.\end{cases} \tag{22}$$

These matching conditions at $r=S$ are analogous to those in the KKR method,[6] with the electron momentum in the interstitial region being equal to zero. The matching conditions take explicitly into account the fact that the off-diagonal elements in the single-site transition matrix are nonzero.[8]

The basic assumption of the itinerant theory of magnetism is that the electrons responsible for magnetic properties are described by Bloch functions. The one-center expansion[7] of the Bloch sum of the free-electron relativistic muffin-tin orbitals $\tilde{X}^{s}_{l\mu}(\mathbf{r})(s=\pm\frac{1}{2})$ in the sphere at $\mathbf{q}'$ has the form

$$\begin{aligned}\tilde{X}^{\mathbf{k},s}_{L\mu}(\mathbf{r}-\mathbf{q}')&=\delta_{\mathbf{q}'\mathbf{q}}\tilde{\phi}^{s}_{L\mu}(-l-1,\mathbf{r}-\mathbf{q}) \\ &\quad+\sum_{\mathbf{R}\neq 0}e^{i\mathbf{k}\cdot\mathbf{R}}\tilde{X}^{s}_{L\mu}(\mathbf{r}-\mathbf{R}-\mathbf{q}') \\ &=\delta_{\mathbf{q}'\mathbf{q}}\tilde{\phi}^{s}_{L\mu}(-l-1,\mathbf{r}-\mathbf{q}) \\ &\quad-\sum_{l's'\mu'}\frac{\tilde{\phi}^{s'}_{L'\mu'}(l',\mathbf{r}-\mathbf{q}')}{2(2l'+1)} \\ &\quad\times\sqrt{\frac{S_{\mathbf{q}}}{S_{\mathbf{q}'}}}\mathcal{S}^{\mathbf{k}}_{L',s',\mu';L,s,\mu}.\end{aligned} \tag{23}$$

Here the subscript L denotes the set $\{\mathbf{q},l\}$; $\mathbf{q}$ is the position of an atom in the unit cell. The relativistic structure constants $\mathcal{S}^{\mathbf{k}}_{L',s',\mu';L,s,\mu}$ are related to the nonrelativistic structure constants $S^{\mathbf{k}}_{L',m';L,m}$ by the expansion in terms of Clebsch-Gordan coefficients[7]

$$\begin{aligned}\mathcal{S}^{\mathbf{k}}_{L',s',\mu';L,s,\mu}&=\sum_{s=\pm 1/2}C^{j',s}_{l',\mu'-s,1/2,s}S^{\mathbf{k}}_{L',m'-s;L,m-s} \\ &\quad\times C^{j,s}_{l,\mu-s,1/2,s}.\end{aligned} \tag{24}$$

Inside a sphere at the site $\mathbf{q}$ the spin-polarized relativistic muffin-tin orbital (SpRMTO) $X^{s}_{L\mu}(\mathbf{r})$ is now given by $\Phi^{s}_{L\mu}(-l-1,\mathbf{r}-\mathbf{q})$. In the interstitial region we assume that $E-V-\beta\boldsymbol{\sigma}\cdot\mathbf{B}$ is zero, and the expression for the SpRMTO

is $\tilde{\phi}^s_{L\mu}(-l-1,\mathbf{r}-\mathbf{q})$. In a sphere centered at a different lattice site $\mathbf{R}+\mathbf{q}'$ it is a linear combination of the functions $\Phi^{s'}_{L'\mu'}(l',\mathbf{r}-\mathbf{R}-\mathbf{q}')$ such that the SpRMTO $X^s_{L\mu}(\mathbf{r})$ is continuous everywhere in the crystal. Then a one-center expansion of the Bloch sum of the SpRMTO's can be constructed. In the sphere at $\mathbf{q}'$ it reads

$$X^{\mathbf{k},s}_{L\mu}(\mathbf{r}-\mathbf{q}')=\delta_{\mathbf{q}'\mathbf{q}}\Phi^s_{L\mu}(-l-1,\mathbf{r}-\mathbf{q})-\sum_{l's'\mu'}\frac{\Phi^{s'}_{L'\mu'}(l',\mathbf{r}-\mathbf{q}')}{2(2l'+1)}\sqrt{\frac{S_{\mathbf{q}}}{S_{\mathbf{q}'}}}\mathcal{S}^{\mathbf{k}}_{L',s',\mu';L,s,\mu}. \tag{25}$$

In terms of the basic functions (25) the trial function is

$$\Psi^{\mathbf{k}}(E^{\mathbf{k}}_i,\mathbf{r})=\sum_{L\mu s}A^{\mathbf{k},s}_{i,L\mu}X^{\mathbf{k},s}_{L\mu}(\mathbf{r}), \tag{26}$$

and the variational problem arising from the crystal Dirac equation leads to the generalized eigenvalue problem

$$\sum_{Ls\mu}(H^{\mathbf{k},s's}_{L'\mu',L\mu}-E^{\mathbf{k}}_i O^{\mathbf{k},s's}_{L'\mu',L\mu})A^{\mathbf{k},s}_{i,L\mu}=0, \tag{27}$$

which is linear in energy since the basis functions do not depend on energy. The diagonalization of this set yields eigenvalues $E^{\mathbf{k}}_i$ and eigenvectors $A^{\mathbf{k},s}_{i,L\mu}$ for a given Bloch vector $\mathbf{k}$ (i is the band number).

The overlap and the Hamiltonian matrices now read

$$\begin{aligned}O^{\mathbf{k},s's}_{L'\mu',L\mu}&=\sum_{\mathbf{q}''}\langle X^{\mathbf{k},s'}_{L'\mu'}(\mathbf{r})|X^{\mathbf{k},s}_{L\mu}(\mathbf{r})\rangle_{\mathbf{q}''}=\delta_{L'L}\delta_{\mu'\mu}\delta_{s's}\langle\Phi^s_{L\mu}(-l-1)|\Phi^s_{L\mu}(-l-1)\rangle\\&-\left[\frac{\langle\Phi^{s'}_{L'\mu'}(-l'-1)|\Phi^{s'}_{L'\mu'}(l')\rangle}{2(2l'+1)}\sqrt{\frac{S_{\mathbf{q}}}{S_{\mathbf{q}'}}}+\frac{\langle\Phi^s_{L\mu}(-l-1)|\Phi^s_{L\mu}(l)\rangle}{2(2l+1)}\sqrt{\frac{S_{\mathbf{q}'}}{S_{\mathbf{q}}}}\right]\mathcal{S}^{\mathbf{k}}_{L',s',\mu';L,s,\mu}\\&+\sqrt{S_{\mathbf{q}'}S_{\mathbf{q}}}\sum_{L''s''\mu''}\frac{1}{S_{\mathbf{q}''}[2l''(l''+1)]^2}\langle\Phi^{s''}_{L''\mu''}(l'')|\Phi^{s''}_{L''\mu''}(l'')\rangle\mathcal{S}^{\mathbf{k}}_{L',s',\mu';L'',s'',\mu''}\mathcal{S}^{\mathbf{k}}_{L'',s'',\mu'';L,s,\mu},\end{aligned} \tag{28}$$

$$\begin{aligned}H^{\mathbf{k},s's}_{L'\mu',L\mu}&=\sum_{\mathbf{q}''}\langle X^{\mathbf{k},s'}_{L'\mu'}(\mathbf{r})|\mathcal{H}|X^{\mathbf{k},s}_{L\mu}(\mathbf{r})\rangle_{\mathbf{q}''}\\&=\delta_{L'L}\delta_{\mu'\mu}\{\delta_{s's}\Phi^s_{L\mu}(-l-1)|\mathcal{H}^0+\mathcal{H}^M_z|\Phi^s_{L\mu}(-l-1)\rangle+(1-\delta_{s's})\langle\Phi^{-s}_{L\mu}(-l-1)|\mathcal{H}^M_z|\Phi^s_{L\mu}(-l-1)\rangle\}\\&-\left\{\left[\frac{\langle\Phi^{s'}_{L'\mu'}(-l'-1)|\mathcal{H}^0+\mathcal{H}^M_z|\Phi^{s'}_{L'\mu'}(l')\rangle}{2(2l'+1)}\sqrt{\frac{S_{\mathbf{q}}}{S_{\mathbf{q}'}}}+\frac{\langle\Phi^s_{L\mu}(-l-1)|\mathcal{H}^0+\mathcal{H}^M_z|\Phi^s_{L\mu}(l)\rangle}{2(2l+1)}\right.\right.\\&\times\left.\sqrt{\frac{S_{\mathbf{q}'}}{S_{\mathbf{q}}}}+\frac{\sqrt{S_{\mathbf{q}'}S_{\mathbf{q}}}}{2}\right]\mathcal{S}^{\mathbf{k}}_{L',s',\mu';L,s,\mu}+\frac{\langle\Phi^{s'}_{L'\mu'}(-l'-1)|\mathcal{H}^M_z|\Phi^{-s'}_{L'\mu'}(l')\rangle}{2(2l'+1)}\sqrt{\frac{S_{\mathbf{q}}}{S_{\mathbf{q}'}}}\mathcal{S}^{\mathbf{k}}_{L',-s',\mu';L,s,\mu}\\&+\left.\frac{\langle\Phi^s_{L\mu}(-l-1)|\mathcal{H}^M_z|\Phi^{-s}_{L\mu}(l)\rangle}{2(2l+1)}\sqrt{\frac{S_{\mathbf{q}'}}{S_{\mathbf{q}}}}\mathcal{S}^{\mathbf{k}}_{L',s',\mu';L,-s,\mu}\right\}+\sqrt{S_{\mathbf{q}'}S_{\mathbf{q}}}\sum_{L''s''\mu''}\frac{1}{S_{\mathbf{q}''}[2l''(l''+1)]^2}\{\langle\Phi^{s''}_{L''\mu''}(l'')|\mathcal{H}^0\\&+\mathcal{H}^M_z|\Phi^{s''}_{L''\mu''}(l'')\rangle\mathcal{S}^{\mathbf{k}}_{L',s',\mu';L'',s'',\mu''}\mathcal{S}^{\mathbf{k}}_{L'',s'',\mu'';L,s,\mu}+\langle\Phi^{-s''}_{L''\mu''}(l'')|\mathcal{H}^M_z|\Phi^{s''}_{L''\mu''}(l'')\rangle\mathcal{S}^{\mathbf{k}}_{L',s',\mu';L,s,\mu}\mathcal{S}^{\mathbf{k}}_{L'',-s'',\mu'';L,s,\mu}\},\end{aligned} \tag{29}$$

$$\mathcal{H}^M_z=\beta\sigma_z B_z(\mathbf{r}). \tag{30}$$

The expression for the matrix elements of the Hamiltonian is much more sophisticated than in the conventional RLMTO method,[7] because they originate from (and have the same symmetry as) the single-site transition matrix $t_{L'\mu',L\mu}$. Its explicit block-diagonal form can be found in Ref. 8. Note that the matrix elements of both $\mathcal{H}^0$ and $\mathcal{H}^M_z$ contribute to the main diagonal of the transition matrix, whereas those of $\mathcal{H}^M_z$ refer to secondary diagonals. So, for an arbitrary wave function $\bar{\varphi}^{s'}_{L'\mu'}(\boldsymbol{\rho}),\underline{\varphi}^s_{L\mu}(\boldsymbol{\rho})$, which has the structure of $\Phi^s_{l\mu}(D,\mathbf{r})$ (21) respective matrix elements read

$$\langle\bar{\varphi}^{s'}_{l'\mu'}(\boldsymbol{\rho})|\underline{\varphi}^s_{l\mu}(\boldsymbol{\rho})\rangle=\delta_{l'l}\delta_{s's}\delta_{\mu'\mu}\int_0^S[\bar{g}^s_{l\mu}\underline{g}^s_{l\mu}+\bar{f}^s_{l\mu}\underline{f}^s_{l\mu}]\rho^2\,d\rho, \tag{31}$$

$$\langle \overline{\varphi}^{s}_{l'\mu'}(\boldsymbol{\rho})|\mathcal{H}^{0}|\underline{\varphi}^{s}_{l\mu}(\boldsymbol{\rho})\rangle$$
$$= \delta_{l'l}\delta_{s's}\delta_{\mu'\mu}\int_0^S \Bigg\{ -\overline{g}^{s}_{l\mu}\left[\frac{d}{d\rho}+\frac{1-\kappa(l,s)}{\rho}\right]c\underline{f}^{s}_{l\mu}$$
$$+c\overline{f}^{s}_{l\mu}\left[\frac{d}{d\rho}+\frac{1+\kappa(l,s)}{\rho}\right]\underline{g}^{s}_{l\mu}+V(\rho)\overline{g}^{s}_{l\mu}\underline{g}^{s}_{l\mu}$$
$$+\left[\frac{V(\rho)}{c^2}-1\right]c^2\overline{f}^{s}_{l\mu}\underline{f}^{s}_{l\mu}\Bigg\}\rho^2\,d\rho, \tag{32}$$

$$\langle \overline{\varphi}^{s}_{l'\mu'}(\boldsymbol{\rho})|\beta\sigma_z B_z|\underline{\varphi}^{s}_{l\mu}(\boldsymbol{\rho})\rangle$$
$$= -\delta_{l'l}\delta_{\mu'\mu}\Bigg\{\delta_{s's}\mu\int_0^S\Bigg[\frac{1}{\kappa(l,s)+\frac{1}{2}}\overline{g}^{s}_{l\mu}\underline{g}^{s}_{l\mu}$$
$$+\frac{1}{\kappa(l,s)-\frac{1}{2}}\overline{f}^{s}_{l\mu}\underline{f}^{s}_{l\mu}\Bigg]B_z(\rho)\rho^2\,d\rho$$
$$-(1-\delta_{s's})\int_0^S\sqrt{1-\left(\frac{\mu}{l+\frac{1}{2}}\right)^2}$$
$$\times\overline{g}^{-s}_{l\mu}\underline{g}^{s}_{l\mu}B_z(\rho)\rho^2\,d\rho\Bigg\}, \tag{33}$$

$$\langle \overline{\varphi}^{s}_{l'\mu'}(\boldsymbol{\rho})|\beta l_z|\underline{\varphi}^{s}_{l\mu}(\boldsymbol{\rho})\rangle$$
$$= \delta_{l'l}\delta_{\mu'\mu}\Bigg\{\delta_{s's}\mu\int_0^S \operatorname{sgn}\kappa(l,s)\Bigg[\frac{\kappa(l,s)+1}{l+\frac{1}{2}}\overline{g}^{s}_{l\mu}\underline{g}^{s}_{l\mu}$$
$$+\frac{\kappa(l,s)-1}{\kappa(l,s)-\frac{1}{2}}\overline{f}^{s}_{l\mu}\underline{f}^{s}_{l\mu}\Bigg]\rho^2\,d\rho$$
$$+(1-\delta_{s's})\frac{1}{2}\int_0^S\sqrt{1-\left(\frac{\mu}{l+\frac{1}{2}}\right)^2}$$
$$\times\overline{g}^{-s}_{l\mu}\underline{g}^{s}_{l\mu}\rho^2 d\rho\Bigg\}. \tag{34}$$

If one neglects $\mathcal{H}^{M}_{z}$ (30) at the stage of solving the set of coupled radial equations then the superscript η in Eqs. (21) and (22) is lost and one comes to the perturbational approach to the spin-polarized RLMTO described in Ref. 1.

$Ls\mu$ component of the crystal wave function (26) in the sphere at $\mathbf{q}$ can be easily obtained by inserting Eq. (25) into Eq. (26) and renaming the subscripts

$$\Psi^{\mathbf{k},s}_{L\mu}(E^{\mathbf{k}}_i,\mathbf{r}) = A^{\mathbf{k},s}_{i,L\mu}\Phi^{s}_{L\mu}(-l-1,\mathbf{r}-\mathbf{q})$$
$$-\frac{\Phi^{s}_{L\mu}(l,\mathbf{r}-\mathbf{q})}{2(2l+1)}\sum_{L's'\mu'}A^{\mathbf{k},s'}_{i,L'\mu'}$$
$$\times\sqrt{\frac{S_{\mathbf{q}'}}{S_{\mathbf{q}}}}\mathcal{S}^{\mathbf{k}}_{L,s,\mu;L',s',\mu'}. \tag{35}$$

The spherically averaged partial contributions to the electronic density and to the z component of the spin moment, which arise in self-consistent calculations, take the form

$$n_{L\mu}(E,\rho) = \frac{\Omega}{(2\pi)^3}\sum_i\sum_{s',s}\int_{BZ}$$
$$\times\left[\frac{1}{4\pi}\int\langle\Psi^{\mathbf{k},s'}_{L\mu}(E^{\mathbf{k}}_i,\boldsymbol{\rho})|\Psi^{\mathbf{k},s}_{L\mu}(E^{\mathbf{k}}_i,\boldsymbol{\rho})\rangle d\hat{\rho}\right]$$
$$\times\delta(E-E^{\mathbf{k}}_i)d\mathbf{k}, \tag{36}$$

$$[m_z]_{L\mu}(E,\rho) = \mu_B\frac{\Omega}{(2\pi)^3}\sum_i\sum_{s',s}\int_{BZ}$$
$$\times\left[\frac{1}{4\pi}\int\langle\Psi^{\mathbf{k},s'}_{L\mu}(E^{\mathbf{k}}_i,\boldsymbol{\rho})|\beta\sigma_z|\Psi^{\mathbf{k},s}_{L\mu}(E^{\mathbf{k}}_i,\boldsymbol{\rho})\rangle d\hat{\rho}\right]$$
$$\times\delta(E-E^{\mathbf{k}}_i)d\mathbf{k}, \tag{37}$$

where E_F is the Fermi energy and Ω is the unit-cell volume.

Noncollinear ordering of the spin moments for arbitrary crystal structures with many atoms per unit cell can be treated as proposed by Ebert.[1]

Finally, note that the proposed formalism has two exact limits: the non-spin-polarized relativistic limit[7] and the spin-polarized nonrelativistic limit. In contrast to other methods developed some years ago,[2,4,3] in the general case the coupling between relativistic effects and intrinsic magnetic field is treated ''on equal footing'' both inside the atomic sphere and in the interstitial region.

III. RELATIVISTIC SPIN-POLARIZED BAND STRUCTURE OF IRON

As an example of the application of the method, we have chosen ferromagnetic iron because its electronic structure is well studied. We have self-consistently calculated the energy bands and the energy distribution of spin, orbital, and total magnetic moments in the bcc iron at the experimental lattice constant 5.405 a.u. The atomic sphere approximation[17] was used, which assumes spherically averaged potential within the Wigner-Zeits sphere of the radius S_{WZ}.

The exchange-correlation potential of von Barth and Hedin[18] without relativistic corrections was used. The set of coupled equations for both the four radial functions and their energy derivatives was solved with two parallel finite-difference schemes. The numerical method is similar to that used in Ref. 6 to construct the spin-polarized relativistic-Korringa-Kohn-Rostoker radial functions. The angular-momentum expansion of the trial function (26) was up to $l=2$.

Figure 1 presents the energy band structure for the spin

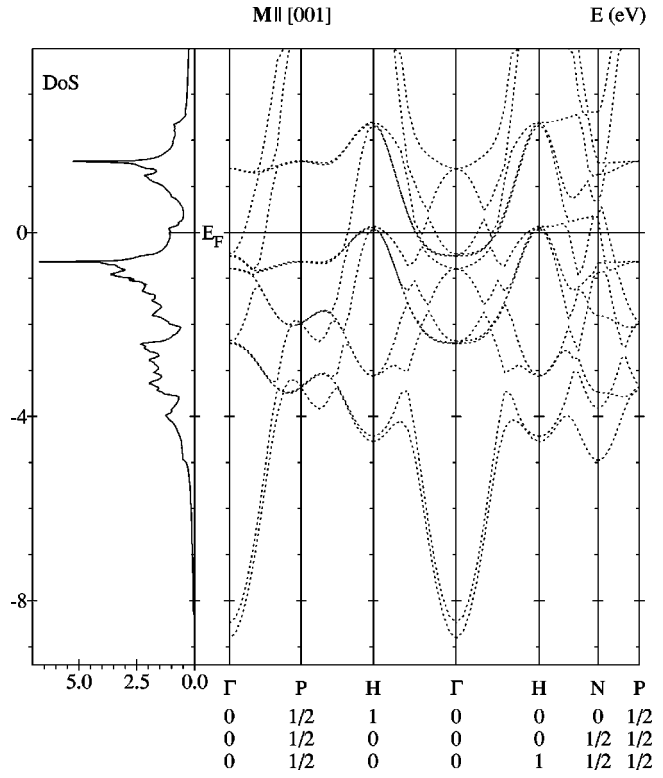

FIG. 1. Energy bands for bcc Fe with the magnetization parallel to [001] and total DOS (in units of states/eV atom).

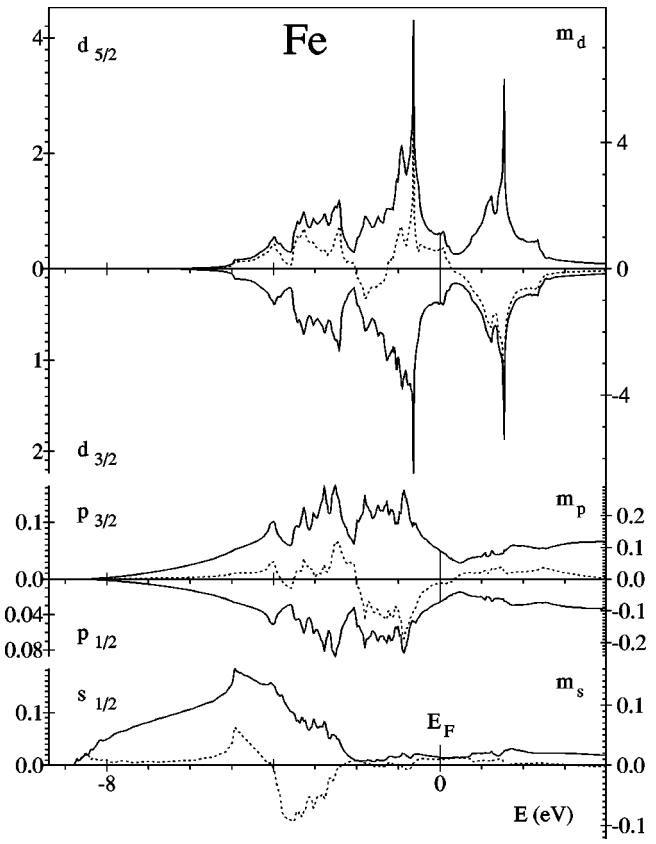

FIG. 2. Partial density of states (solid curves, scale at the left in units of states/eV atom) and partial densities of spin magnetization (dashed curves, scale at the right in units of μ_B/eV atom) for bcc Fe with the magnetization parallel to [001].

alignment parallel to the [001] direction. The presence of the magnetic field together with the spin-orbit coupling lowers the point symmetry so that the irreducible wedge of the Brillouin zone (IBZ) comprises 1/16 of the BZ. The geometry of the IBZ can be found in Ref. 19. The total and κ-projected partial DOS's and l-projected partial densities of spin magnetization were calculated using the tetrahedron method with a uniform sampling of 1261 **k** points in the IBZ. The notation of the high-symmetry points shown in Fig. 1 refers to the 1/48 of the BZ. Core states were treated self-consistently by solving the full non-spin-polarized Dirac equation for the crystal potential. $3d$, $4s$, and $4p$ states were treated as valence bands. The self-consistency criterion — i.e., the integral over atomic sphere of the absolute value of the difference between the input and the output (charge and spin) densities — was chosen to be $10^{-4}e$. Our bands agree with those reported earlier.[20–22] The (l,j) resolved DOS functions are given in Fig. 2 (note that presented are *not* spin-up and spin-down DOS's). The DOS at the Fermi energy $N(E_F)$ is given in Table I.

The exchange splitting of the P_4 was 1.345 eV; the value is in reasonable agreement with the experimental value[23] of 1.5 eV. The calculated value of $N(E_F)$ agrees well with the values reported in Ref. 21 but it is approximately half of the experimental value (see the discussion in this reference).

Another important quantity is the partial densities of spin magnetization $m_l(E)$, that is an integral of $[m_z]_{L\mu}(E,\rho)$ [see Eq. (37)] over the atomic sphere. Figure 2 displays its energy dependence in the energy range from the bottom of the valence band up to 4 eV above E_F. As expected, the d contribution is much larger than those from other angular momenta. Figure 1 shows that over the occupied part of the spectrum the d states have predominantly positive (spin-up) spin-magnetization $m_d(E)$, but at 0.3 eV above E_F it changes sign and is strongly negative (spin-down) up to 3 eV. Table II presents the calculated and the experimental spin and orbital moments. The theoretical values are close to those based on the full-potential LMTO method[25] within the LSDA framework, which exploited a perturbational treatment of relativistic effects. The calculated orbital moment is slightly smaller than the experimental value because of our neglecting the orbital polarization effects in the Hamiltonian (2).

IV. ELECTRONIC STRUCTURE OF Fe-Ni ALLOYS AT THE INNER EARTH'S CORE CONDITIONS

In this section we apply the method to the calculation of the ordered simple cubic close-packed $FeNi_3$ (see the Introduction). Details of the band-structure calculations are presented in the beginning of Sec. III. Owing to the strong compression of the crystal lattice, the BZ volume increases and

TABLE I. Angular-momentum-projected $N(E_F)$ (in units of states/Ry) for bcc Fe, $M\|[001]$.

$s_{1/2}$	$p_{1/2}$	$p_{3/2}$	$d_{3/2}$	$d_{5/2}$	Σ	Expt.[a]
0.20	0.35	0.68	5.13	8.25	14.61	27.37

[a]Reference 24.

TABLE II. Angular-momentum decomposed spin and orbital magnetic moments (in units of μ_B) for bcc Fe, $M \| [001]$.

	M_{spin}				M_{orb}				M_{total}
	s	p	d	Σ	s	p	d	Σ	
Theor.	−0.014	−0.059	2.280	2.206	0.000	0.000	0.049	0.049	2.255
Expt.[a]				2.13				0.08	2.21

[a]Reference 26.

the valence band broadens. We used 1547 points in the IBZ, which for the [111] direction of magnetization comprised 1/12 of the BZ. The self-consistency criterion was chosen $10^{-5}e$. That choice of parameters is necessary to ensure the convergence of the self-consistent procedure in total energy. The atomic sphere radii were chosen equal, $S_{\mathrm{Fe}}=S_{\mathrm{Ni}}=2.285$ a.u.

It is well known that the gradient corrections to the LSDA do not strongly affect the band energies and the spin magnetization, but they are important for the total energy.[11] Moreover, as has been pointed out in Ref. 20 at smaller volumes the charge-density gradient is, in general, smaller. In addition, we believe that the nonsphericity of the spatial distribution of the electron- and spin-magnetization densities should be small because of the enhancement of the *d* electron delocalization under the pressures considered. These assumptions significantly simplify the computer simulation; the errors they introduce are evidently less than the error due to the uncertainties in chemical composition and crystal structure. We believe that these assumptions do not considerably affect the ultimate results.

Non-spin-polarized scalar-relativistic electronic structure calculations for the ground state of some stoichiometric $\mathrm{Fe}_{1-x}\mathrm{Ni}_x$ compounds with several values of the concentration of Fe have been performed. The DOS's of the constituent atoms are shown in Fig. 3. Here FeNi and $\mathrm{Fe_3Ni}$ compounds were chosen to possess a simple cubic lattice originating from the fcc structure, and the unit cell of $\mathrm{Fe_7Ni}$ was assumed to consist of two Fe fcc cubic cells with one Fe atom replaced by Ni. The lattice constants of all of these alloys were chosen to provide the same mass density ($13\ \mathrm{g/cm^3}$). Of course, the gross features of the total DOS are determined by the *d* contribution. (The *l* decompositions of the functions are not shown.) When the lattice is compressed the *d* band is expected to broaden owing to the enhanced overlap of neighboring orbitals. However, Fig. 3 displays an interesting trend when the concentration of Ni is increased: the Fe *d* bands become narrower and $N(E)$ grows. Moreover, the compound $\mathrm{FeNi_3}$ [plot (e)] exhibits, firstly, a distinct peak in the filled valence band in the vicinity of the Fermi level, and, secondly, a sizable Fe-DOS at E_F, $N(E_F)=2.53$ states/eV atom. This situation is similar to those in non-spin-polarized calculations for Fe, Co, and Ni at the ambient pressure, where $N(E_F)$ values lie in the range from 2 to 4 states/eV atom.[27]

This unusual effect can be understood in the following way. Calculations that neglect the hybridization between iron and nickel electron orbitals (not reported here) demonstrate that the lower part of the valence band, $E-E_F<-1$ eV, originates mostly from the Ni *d* states. The Fe *d* states form a narrow band (a half-width of 2 eV), which is partially occupied. Though the distance between neighboring Fe atoms in that alloy (5.847 a.u., i.e., the lattice constant) is larger than that in the bcc Fe under the ambient pressure (4.680 a.u.), it should be noted that the distance between neighboring Fe and Ni atoms is only 4.135 a.u. The Fe $3d$ electrons are affected by strong repulsive potential of the Ni sphere and vice versa, and atomic spheres of each sort of atoms is weakly transparent for the electrons of the other sort. The increase of $N(E_F)$ is directly connected with this effect.

The quantity $I(E_F)N(E_F)$, where $I(E_F)$ is the Stoner parameter, is well known to provide a direct criterion of ferromagnetic ordering, which makes it necessary to perform a spin-polarized band-structure calculation of the ground state of this compound. In addition, under the extreme compression the valence electrons move closer to the nuclei and their kinetic energy increases so that the relativistic effects become important.

We have chosen the magnetization along the [111] direction similar to the ordered $\mathrm{FeNi_3}$ at normal conditions, where the easy axis of magnetization is [111] (Ref. 14). Figure 4 represents the energy bands along the high-symmetry direc-

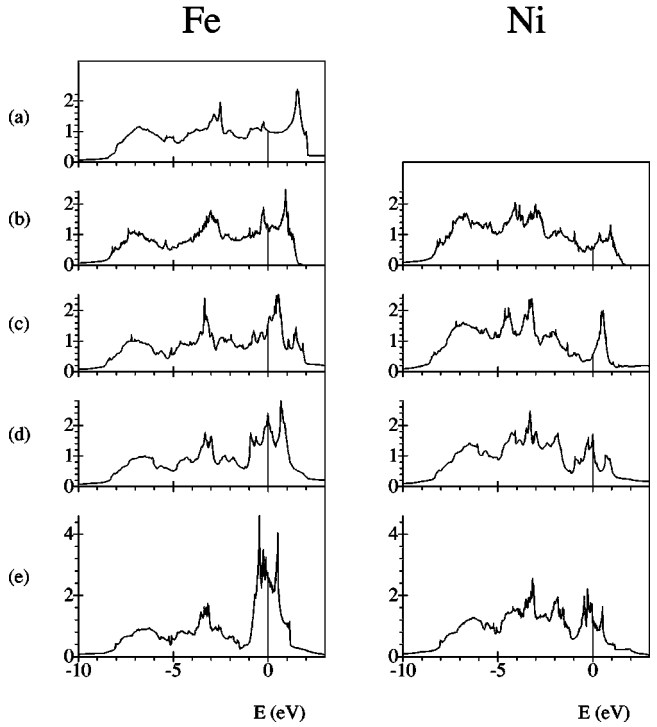

FIG. 3. Non-spin-polarized Fe and Ni DOS's (in units of states/eV atom) for some ordered Fe-Ni compounds with several concentration of Fe but with the same mass density ($13\ \mathrm{g/cm^3}$): (a) fcc Fe, (b) $\mathrm{Fe_7Ni}$, (c) $\mathrm{Fe_3Ni}$, (d) FeNi, (e) $\mathrm{FeNi_3}$ (see text).

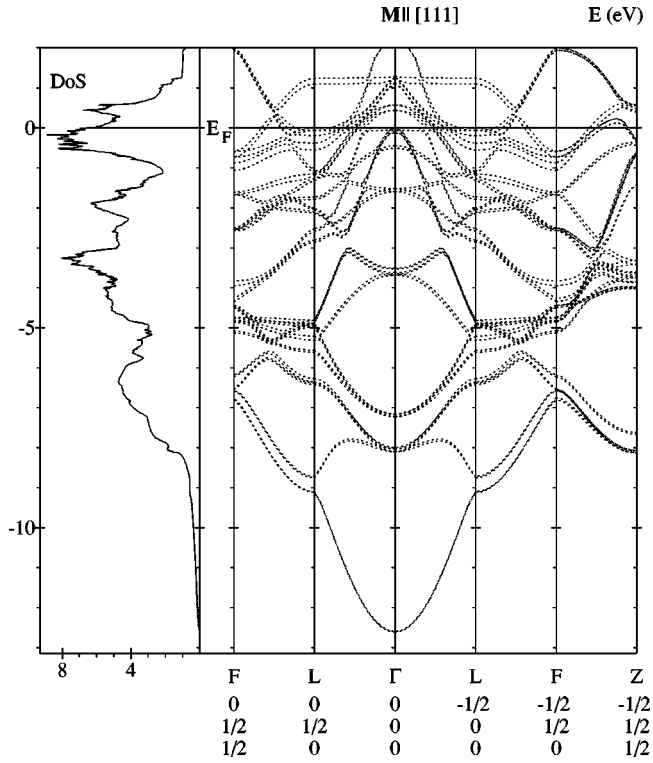

FIG. 4. Energy bands for $FeNi_3$ with the magnetization along [111] and total DOS (in units of states/eV atom).

tions and the total DOS at the lattice parameter considered. The partial DOS's and the energy dependence of the spin magnetization are shown in Fig. 5, which shows that the d contribution strongly dominates. Moreover, the $d(\mu=\pm\frac{5}{2})$ states mainly contribute to the $m_d(E)$ in the vicinity of the Fermi level. In addition, Table III presents calculated values of integral magnetic properties together with the angular momentum decomposition of the spin and orbital magnetic moments of components. The table indicates that both spin and orbital moments are mainly concentrated at the Fe site because the E_F falls at the peak of the nonmagnetic Fe DOS [see Fig. 3(e)]. However, the three Ni atoms contribute considerably to the resulting magnetization.

Owing to the relatively small spin polarization obtained, the total DOS is similar to that with the spin polarization turned off. Additionally, the value of $N(E_F)$ remains sufficiently large (see Table IV). That may be a source of magnetic instabilities, which occur, for instance, in $3d$-rich ternary compounds $R_2Fe_{14}B$ and $R_2Co_{14}B$, where R is a heavy rare-earth element.[28] Note that in such a case each sublattice may favor different easy magnetization directions and the increase of the temperature may result in the spin-reorientation phenomena.

Special attention is paid to the energy dependence of the spin polarization of d states of the alloy components (Fig. 5). This range is characterized by a very strong oscillatory behavior of $m(E)$. The contribution from the bottom of the valence band up to 2 eV below E_F to the resulting magnetization is nearly zero for both components. Moreover, the main contribution to the integral cell moment comes from the distinct peak at 0.8 eV below E_F, though in the immediate vicinity of E_F $m(E)$ is negative. It should be noted, however, that, as is seen from Fig. 3, the situation differs from that in iron under normal conditions, where the Fermi level lies at the high energy edge of the respective peak, but is rather similar to that in nickel (see, e.g., Ref. 29).

The decrease of the total energy of the crystal due to the spin alignment is found to be 0.012 eV; this value should not be considered exact because of the use of the LSDA. It is surprising that, in contrast to the close-packed phases of pure Fe under the high pressure,[11] the spin alignment turns out to be favorable at the 1.5-fold compression of the lattice.

Should the IC be made only of the $FeNi_3$ compound at zero temperature, then the theoretically predicted magnetic properties of this compound would lead to the value of the Earth's magnetic field 12.3 times greater than the experimentally observed value.

As far as the influence of the structural ordering on the magnetization is concerned, it should be noted that under normal conditions the mean field in the disordered $FeNi_3$ is larger than in the ordered state,[14] although direct analogy between the strongly compressed and the normal state may be inconsistent.

Some additional remarks should be made on the peculiarities of the picture of the ferromagnetic ordering suggested by the present theory. It is generally accepted that transition metals do not manifest magnetic behavior at extreme pressures (i.e., at very small atomic volumes) because the d states become smeared over the wide valence band. Thereby the DOS at the Fermi level, $N(E_F)$, becomes rather small, and distinct DOS peaks near the Fermi level disappear. Such a behavior is illustrated by Fig. 3. All the curves (a)–(d) are smooth and have no pronounced peaks. Thus a ferromagnetic alignment should not be expected in these stoichiometric compounds, which has been confirmed by our SpRLMTO calculation: we did not observe a sizable ferromagnetism in FeNi. In contrast to that, $Fe_{1-x}Ni_x$ alloys with $x>0.26$ are ferromagnetic under ambient pressure (Ref. 15). Neglecting the possibility of the antiferromagnetic or spiral spin alignment one may conclude that the strongly compressed $FeNi_3$ compound demonstrates a pure itinerant (weak) ferromagnetism that originates only from the valence band structure without any localized moments due to the exchange-correlation interaction on a $3d$-metal site.[30]

Although a spin-polarized band theory coming from the

TABLE III. Calculated angular-momentum decomposed spin and orbital magnetic moments (in units of μ_B) for $FeNi_3$, $M\|[111]$.

Atom	M_{spin}				M_{orb}				M_{total}
	s	p	d	Σ	s	p	d	Σ	
Fe	0.001	0.001	0.206	0.208	0.000	0.000	0.011	0.011	0.219
Ni	0.001	−0.002	0.058	0.057	0.000	0.000	0.001	0.001	0.058

TABLE IV. Calculated angular-momentum decomposed $N(E_F)$ (in units of states/eV atom) for $FeNi_3$, $M \| [111]$.

Atom	$s_{1/2}$	$p_{1/2}$	$p_{3/2}$	$d_{3/2}$	$d_{5/2}$	Σ
Fe	0.01	0.02	0.03	0.97	1.61	2.64
Ni	0.01	0.01	0.03	0.45	0.75	1.25

Stoner theory provides a satisfactory description of the magnetic properties of transition metals at very low temperatures, it fails to account for the magnetic properties at finite temperatures, first of all for the Curie temperature T_C. T_C appears to be too high because of the neglect of orientational spin fluctuations of local magnetization, which must be taken into account in a realistic finite-temperature theory.[30,34,31]

However, it turns out that the Stoner theory has an attractive feature to overestimate T_C in a regular manner, at least for Fe, Co, and Ni,[32,31] that is the ratio T_C^{St}/T_C lies in the range from 3 to 6 (about 4.7 for Ni). This enables us to apply a generalization of the Kohn-Sham theory proposed by Eckardt and Fritsche,[29,33] which reduces to a Stoner-like theory for realistic charge and spin densities. Moreover, it has been pointed out by Staunton and Gyorffy[31] that nickel can be analyzed in terms of the Stoner theory, although the spin fluctuations lower considerably T_C. In addition, the spin density distribution in $FeNi_3$ (see Fig. 2) is rather similar to that in pure Ni.[27] Within this approach we can rewrite Eqs. (36) and (37) as

$$n(\rho)=\int \sum_{L,\mu} n_{L\mu}(E,\rho) f(T,\zeta,E)\,dE, \tag{38}$$

$$m_z(\rho)=\int \sum_{L,\mu} [m_z]_{L\mu}(E,\rho) f(T,\zeta,E)\,dE, \tag{39}$$

where $f(T,\zeta,E)$ is the Fermi distribution function at the temperature T. The chemical potential ζ is implicitly determined by

$$N=\int n(\rho)\,d\boldsymbol{\rho}, \tag{40}$$

where N is the total number of electrons.

Self-consistent SpRLMTO calculations for the ordered $FeNi_3$ at the same value of lattice parameter have been performed for $T=3000$ K and the resulting magnetic moment of $0.0476\mu_B$ per unit cell was found. This is about $\frac{1}{7}M(T=0)$. Assuming the Brillouin behavior of the magnetization $M(T)$ one can easily estimate T_C^{St} to be slightly larger than 3000 K, so that T_C should lie in the range from 500 K to 1000 K (one would rather expect 600 K assuming the fitting factor to be the same as for Ni, i.e., 4.7). Taking into account a small zero-temperature magnetization, this is an unusual effect, which can be brought out in a more clear way as follows. According to the Stoner theory T_C^{St} is defined by the relation

$$I(E_F)\int \frac{\partial f(T_C^{St},E_F,E)}{\partial E} N(E)\,dE+1=0, \tag{41}$$

where $N(E)$ is a non-spin-polarized DOS. Because the Fermi distribution function at a finite temperature T changes considerably only within an interval of about $\pm kT$ around the Fermi level E_F, the integration is restricted to this energy

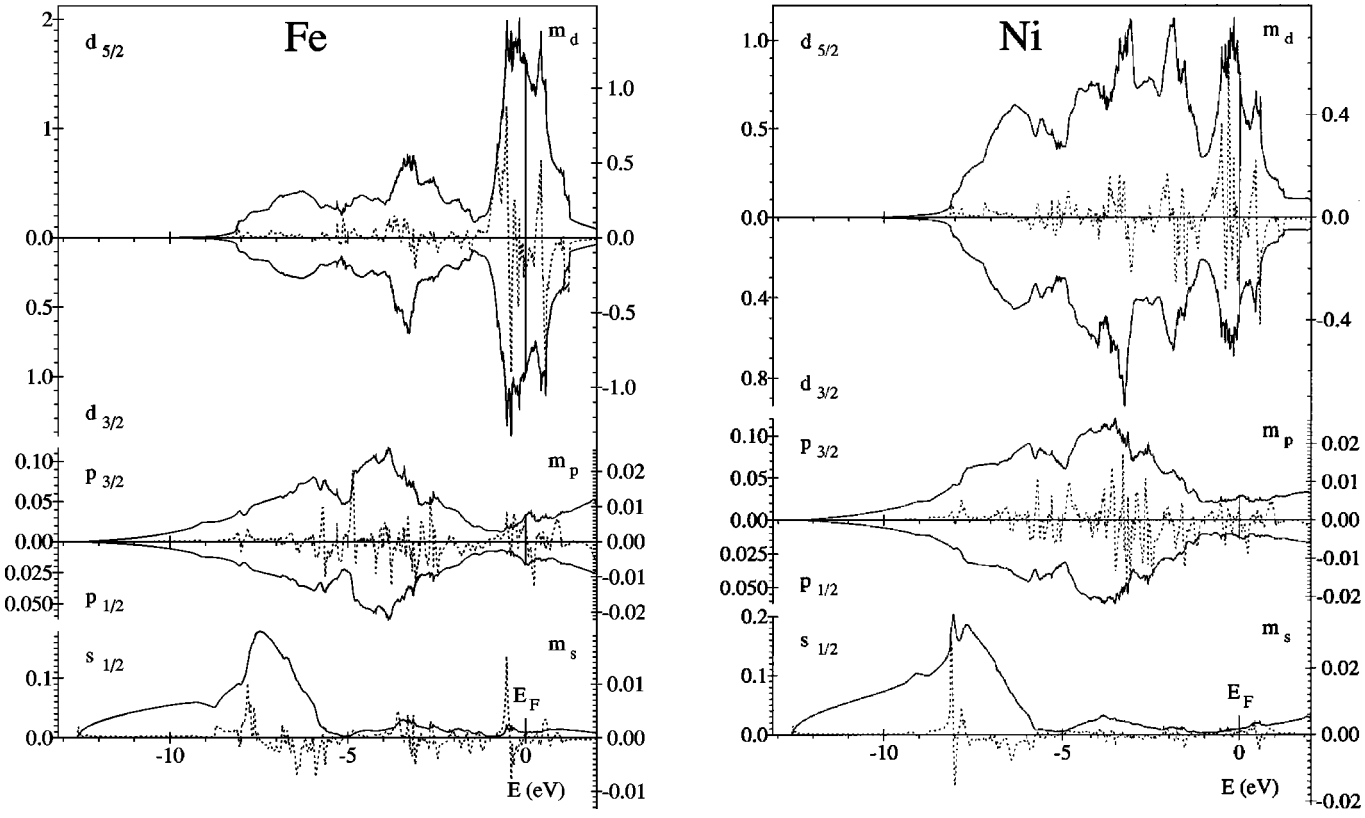

FIG. 5. Partial density of states (solid curves, scale at the left in units of states/eV atom) and partial densities of spin magnetization (dashed curves, scale at the right in units of μ_B/eV atom) for $FeNi_3$ with the magnetization directed along [111].

interval. In contrast to Fe, Co, and Ni (Ref. 27), in spite of the spin polarization turned on the $N(E)$ remains large over the whole interval, and the integral in Eq. (41) diminishes slowly with increasing the temperature parameter. Note that the Stoner parameter $I(E_F)$ that describes the exchange-correlation interaction is assumed to be temperature independent.

It is well known that when the pressure increases the electron gas interacting both with itself and with the nuclei becomes closer to the ideal gas. Let λ be a characteristic length of the structure (e.g., a lattice parameter or a mean distance between electrons). It is clear that the potential energy of electrons is proportional to $1/\lambda$, and the kinetic energy is proportional to $1/\lambda^2$ (because of the Heisenberg relation $\Delta x \Delta p \simeq \hbar$). Thus the ratio of kinetic to potential energy is proportional to $1/\lambda$, and when λ decreases, the electron gas moves towards the ideal gas. Since the Stoner model does not explicitly take into consideration the electron interactions (thereby exploiting the concept of ideal gas of free electrons) it may be expected that under extreme pressures the above ratio would be less than 5 and the actual T_C may be larger than the estimate obtained.

In principle, it would be possible to estimate T_C more accurately using more realistic approaches (see, e.g., Refs. 31 and 34) however, such approaches involve a number of experimental parameters.

V. CONCLUSION

An improved fully relativistic spin-polarized first-principles linear muffin-tin orbital (SpRLMTO) method for density functional theory electronic structure calculations of magnetic crystals containing heavy elements has been developed. This method is based on an internally consistent approach to the basis functions construction, and it possesses all the properties of the conventional methods, both the RLMTO and the spin-polarized LMTO. Using a more accurate solution of the Dirac equation in the presence of magnetic field made it unnecessary to resort to further assumptions and simplifications.

The method has been numerically studied by means of *ab initio* self-consistent calculations of the electronic structure of iron and the results obtained are in excellent agreement with previous theoretical and experimental results.

In particular, the progress achieved in the present paper in *ab initio* describing ferromagnetic order under extreme pressure is demonstrated by the results on the ordered $FeNi_3$ alloy, which may be a possible candidate for the chemical composition of the IC. Although no relevant experiment is likely to be feasible, the calculations give strong evidence that under the conditions assumed intrinsic spin ordering occurs with the resulting magnetic moment of $0.393\mu_B$/cell at least at $T=0$. Though the validity of this model of the IC layer essentially depends on the assumptions used in its construction, we can suggest a unified description of some interesting geophysical data and suggests a coherent understanding of the structure of the Earth's interior.

With these initial results from our self-consistent band-structure calculation of the $FeNi_3$ compound an attempt has been made to bring together the solid state and the geophysical data. However, as only one alloy has been found to exhibit ferromagnetic spin alignment, the above assumptions about real magnetic state of the IC are speculative. Furthermore, several model improvements, which could improve the results and conclusions, are required to produce a more realistic picture in the future. For example, a more detailed thermodynamics including phonon and disorder effects is desirable. On the other hand, the effects of the variation of the chemical composition, crystal structure, density of the IC, and noncollinear spin ordering should also reveal new interesting features. In addition, it would be particularly interesting to elucidate the effect of the lowering of the symmetry of the lattice (within the close-packed crystal structures) on the itinerant magnetism as well as on the elastic anisotropy of the Earth's core,[35] which has not yet been explained.

ACKNOWLEDGMENTS

I am pleased to acknowledge several helpful discussions with Professor E. D. Belokolos. A part of this work concerning the study of the inner Earth's core structure has been funded by the International Research Project ''Warning.''

[1] H. Ebert, Phys. Rev. B **38**, 9390 (1988).
[2] B.C.H. Krutzen and F. SpringelKamp, J. Phys.: Condens. Matter **1**, 8369 (1989).
[3] L. Fritsche, J. Noffke, and H. Eckardt, J. Phys. F **17**, 943 (1987).
[4] S.A. Ostanin and V.P. Shirokovskii, J. Phys.: Condens. Matter **2**, 7585 (1990).
[5] R. Feder, F. Rosicky, and B. Ackermann, Z. Phys. B **52**, 31 (1983).
[6] P. Strange, J. Staunton, and B.L. Gyorffy, J. Phys. C **17**, 3355 (1984).
[7] V.V. Nemoshkalenko, A.E. Krasovskii, V.N. Antonov, Vl.N. Antonov, U. Fleck, H. Wonn, and P. Ziesche, Phys. Status Solidi B **120**, 283 (1983).
[8] G. Schadler, P. Weinberger, A.M. Boring, and R.C. Albers, Phys. Rev. B **34**, 713 (1986).
[9] M.H.P. Bott, *The Interior of the Earth* (Arnold, London, 1971); J.P. Poirier, *Introduction to the Physics of the Earth's Interior* (Cambridge University Press, Cambridge, England, 1991).
[10] *High-Pressure Science and Technology—1993*, edited by S.C. Schmidt, J.W. Shaner, G.A. Samara, and M. Ross (AIP, New York, 1994), pp. 887–966.
[11] P. Söderlind, J.A. Moriarty, and J.M. Wills, Phys. Rev. B **53**, 14 063 (1996).
[12] H.K. Mao, Y. Wu, L.C. Chen, J.F. Shu, and A.P. Jephcoat, J. Geophys. Res. **95**, 21 737 (1990).
[13] L.V. Altshuler, Usp. Fiz. Nauk **85**, 197 (1965) [Sov. Phys. Usp. **8**, 52 (1965)].
[14] T.E. Cranshaw, J. Phys. F **17**, 967 (1987).
[15] *Physics and Applications of Invar Alloys*, Honda Memorial Series on Materials Science No. 3 (Maruzen Company, Tokyo, 1978).
[16] A.H. MacDonald and S.H. Vosko, J. Phys. C **12**, 2977 (1979).
[17] O.K. Andersen, Phys. Rev. B **12**, 864 (1975).

[18] U. von Barth and L. Hedin, J. Phys. C **5**, 1629 (1972).
[19] P. Strange, H. Ebert, J. Staunton, and B.L. Gyorffy, J. Phys.: Condens. Matter **1**, 2959 (1989).
[20] T.C. Leung, C.T. Chan, and B.N. Harmon, Phys. Rev. B **44**, 2923 (1991).
[21] D.J. Singh W.E. Pickett, and H. Krakauer, Phys. Rev. B **43**, 11 628 (1991).
[22] B. Barbiellini, E.G. Moroni, and T. Jarlborg, J. Phys.: Condens. Matter **2**, 7597 (1990).
[23] D.E. Eastman, F.J. Himpsel, and J.A. Knapp, Phys. Rev. Lett. **44**, 95 (1980).
[24] M. Dixon, F.E. Hoare, T.M. Holden, and D.E. Moody, Proc. R. Soc. London, Ser. A **255**, 561 (1965).
[25] J. Trygg, B. Johansson, O. Eriksson, and J.M. Wills, Phys. Rev. Lett. **75**, 2871 (1995).
[26] M.B. Stearns, in *Magnetic Properties of* 3*d*, 4*d and* 5*d Elements, Alloys and Compounds*, edited by K.-H. Hellwege and O. Madelung, Landolt-Börnstein, New Series, Group III, Vol. 19, pt. a (Springer, Berlin, 1987).
[27] V.L. Moruzzi, J.F. Janak, A.R. Williams, *Calculated Electronic Properties of Metals* (Pergamon, New York, 1978).
[28] *Ferromagnetic Materials. A Handbook on the Properties of Magnetically Ordered Substances*, edited by E.P. Wohlfarth and K.H.J. Buschow (North-Holland, Amsterdam, 1988), Vol. 4, pp. 1–130.
[29] H. Eckardt and L. Fritsche, J. Phys. F **17**, 925 (1987).
[30] T. Morya, *Spin Fluctuations in Itinerant Electron Magnetism* (Springer, Berlin, 1985).
[31] J.B. Staunton and B.L. Gyorffy, Phys. Rev. Lett. **69**, 371 (1992).
[32] O. Gunnarsson, J. Phys. F **6**, 587 (1976).
[33] L. Fritsche, Phys. Rev. B **33**, 3976 (1986).
[34] M. Uhl and J. Kübler, Phys. Rev. Lett. **77**, 334 (1996).
[35] J. Tromp, Nature (London) **366**, 678 (1993).